High Valence M-incorporated PdCu nanoparticles (M = Ir, Rh, Ru) for water electrolysis in alkaline solution

Yingnan Qin[# 1], Zuochao Wang[# 1], Wenhao Yu[1], Yingjun Sun[1], Dan Wang[1], Jianping Lai[1], Shaojun Guo[* 3] and Lei Wang[* 1,2]*

[1] Key Laboratory of Eco-chemical Engineering, Key Laboratory of Optic-electric Sensing and Analytical Chemistry of Life Science, Taishan Scholar Advantage and Characteristic Discipline Team of Eco Chemical Process and Technology, College of Chemistry and Molecular Engineering, Qingdao University of Science and Technology, Qingdao 266042, P. R. China

[2] Shandong Engineering Research Center for Marine Environment Corrosion and Safety Protection, College of Environment and Safety Engineering, Qingdao University of Science and Technology, Qingdao 266042, P. R. China

[3] Department of Materials Science & Engineering, College of Engineering, Peking University, Beijing, 100871, China.

[*]E-mail: inorchemwl@126.com (Lei Wang); jplai@qust.edu.cn (Jianping Lai); guosj@pku.edu.cn (Shaojun Guo)

EXPERIMENTAL SECTION

Chemicals. Palladium (II) acetylacetonate ($Pd(acac)_2$, 97%), copper (II) acetylacetonate ($Cu(acac)_2$, 97%), iridium (III) 2,4-pentanedionate ($Ir(acac)_3$, 99%), Ruthenium (III) acetylacetone ($Ru(acac)_3$, 99%), Rhodium (III) 2,4-pentanedionate ($Rh(acac)_3$, 99%), oleylamine (OAm, 70%) and perchloric acid ($HClO_4$, 70%) were all purchased from Sigma-Aldrich. Ascorbic acid (AA, reagent grade) was obtained from Beijing J&K technology co., LTD. Iron (III) chloride hexahydrate ($FeCl_3 \cdot 6H_2O$, reagent grade), hexane, ethanol and isopropanol were purchased from Beijing Tongguang Fine Chemicals Company. All the chemicals were used without further purification, and the solutions were freshly prepared with deionized water (18.2 MΩ/cm).

Synthesis of Ir-PdCu NPs. 7.6 mg $Pd(acac)_2$, 6.5 mg $Cu(acac)_2$, 12 mg $Ir(acac)_3$, 5.4 mg $FeCl_3 \cdot 6H_2O$, 35.6 mg AA and 5 mL OAm were mixed together into a 20 mL glass vial, the solution became clear after sonicating for 1 h. The resulting solution was then heated at 220 °C for 5 h in an oil bath. The resulting colloidal products were collected by centrifugation and washed three times with an ethanol/cyclohexane mixture. The synthesis of Ir_8-PdCu and Ir_{18}-PdCu were similar to Ir_{16}-PdCu, except the usage of $Ir(acac)_3$ was changed to 6 mg and 18 mg.

Synthesis of PdCu NPs. The synthetic procedure for PdCu NPs was similar to that of Ir-PdCu NPs, except the addition of $Ir(acac)_3$.

Synthesis of PdCuIr NPs. The synthesis of PdCuIr was similar to Ir_{16}-PdCu, except the addition of $FeCl_3 \cdot 6H_2O$.

Synthesis of M-PdCu NPs. The synthesis of M-PdCu was similar to Ir_{16}-PdCu. For Rh-PdCu, we

used 12 mg $Rh(acac)_3$ as the substitute for $Ir(acac)_3$. For Ru-PdCu, we used 12 mg $Ru(acac)_3$ to take the place of $Ir(acac)_3$.

Characterization. Transmission electron microscopy (TEM) was conducted on HITACHI HT7700 at an acceleration voltage of 100 kV. High-resolution transmission microscopy (HRTEM) images and energy dispersive X-ray spectroscopy (EDS) were taken by HITACHI SU-8010. The sample dispersed in cyclohexane was dropped onto carbon-coated molybdenum TEM grids using pipettes and dried naturally under ambient condition. Powder X-ray diffraction (XRD) spectra were recorded on an X'Pert-Pro X-ray powder diffractometer equipped with a Cu radiation source (λ = 0.15406 nm). The chemical valence of each element was collected by X-ray photoelectron spectra (XPS) on SSI SProbe XPS Spectrometer. The composition of as-prepared samples was collected by the inductively coupled plasma-atomic emission spectroscopy (ICP-AES, Agilent 8800).

Electrochemical measurements. The as-prepared samples were loaded on carbon (Vulcan XC-72) by sonicating in cyclohexane for 2 h. The catalysts were collected by centrifugation with ethanol for three times. The products were dried at 50 ℃ oven and annealed at 220 ℃ for 2 h to remove the redundant organic surfactant around the surface. The as-prepared catalysts were dispersed into the mixture of deionized water, isopropanol and Nafion solution (v: v: v 1: 1: 0.0025) respectively, the resulting homogeneous 1 mg mL^{-1} inks were obtained after sonicating for around 1 h.

All the electrochemical tests were conducted on CHI 660e electrochemical workstation (Chenhua, Shanghai). A graphite rod electrode, saturated calomel electrode (SCE) and glassy carbon rotating disk electrode (RDE) (diameter: 5 mm, area: 0.196 cm^2) were used as counter electrode, reference electrode and working electrode, respectively. 10 μL of the inks was dropped onto the RDE, in which the Ir loading mass on RDE was 1.07 μg for Ir_{16}-PdCu/C based on ICP-AES analysis.

HER and OER test. The HER and OER performance were tested in N_2 and O_2-saturated 0.1 M $HClO_4$ or 0.1 M KOH, respectively. Before every test, the catalyst modified GCE was activating by cycling at -0.2-1.1 V (vs RHE) at 500 mV s^{-1} for 100 cycles. The polarization curves were conducted at a scan rate of 5 mV s^{-1} with 95 % iR drop compensation, and the chronoamperometry was measured at a constant potential to record the change of current density in 5000 s.

Turnover frequency (TOF). The TOF value was calculated by assuming 100% faradaic efficiency from the following equation: $TOF = j \cdot A / (n \cdot F \cdot N)$. Here, j is the current density under a certain overpotential with 95% iR-compensation (mA cm^{-2}), n is the electron transfer number of the reaction process (2 for HER or 4 for OER), F is Faradic constant (96485 C), N is the moles number of the active component in catalyst and could be calculated by $N = Q_H / nF$. Here, Q_H is integral area of H adsorption peak in acid CV curves.[1].

DFT Calculation: DFT calculations of CuPd and CuPdIr slabs were computed by using using Vienna ab initio simulation package (VASP) within a generalized gradient approximation (GGA) of exchange-correlation functional in the Perdew, Burke, and Ernzerhof (PBE). And GGA+U functional was used with an additional Coulomb potential U = 2.5 eV (Cu), 2.9 eV (Pd) and 2.1 eV (Ir) applied on states of d-orbit. A plane-wave energy cut off of 400 eV was used together with norm-conserving pseudopotentials, and the Brillouin zone was sampled with a 2 × 2 × 1 Monkhorst–Pack grid. The structure was fully optimized until the force on each atom is less than 10^{-3} eV/Å. To avoid periodic interaction, a vacuum layer of 20 Å was incorporated into the slabs. The free energy (G) was computed from $G = E + ZPE - T\Delta S$. Where E was the total energy, ZPE was the zero-point energy, the entropy (ΔS) of each adsorbed state were yielded from DFT calculation, whereas the thermodynamic corrections for gas molecules were from standard tables.

Overall water splitting test. The overall water splitting tests were conducted in a two-electrode system at 0.1 M KOH. The catalyst inks were dropped on 1*1 cm carbon fiber paper (CFP) with a loading mass of 20 μg cm^{-2}. Before the polarization curve test, the surfaces of the catalysts were cleaned by cyclic voltammetry between 1.0 V and 1.6 V (vs RHE) at 500 mV s^{-1} for 100 cycles. Durability tests of overall water splitting were performed by chronoamperometry at a constant potential to record the change of current density in 10 h. The chronopotentiometry tests were conducted at 10 mA for 10 h.

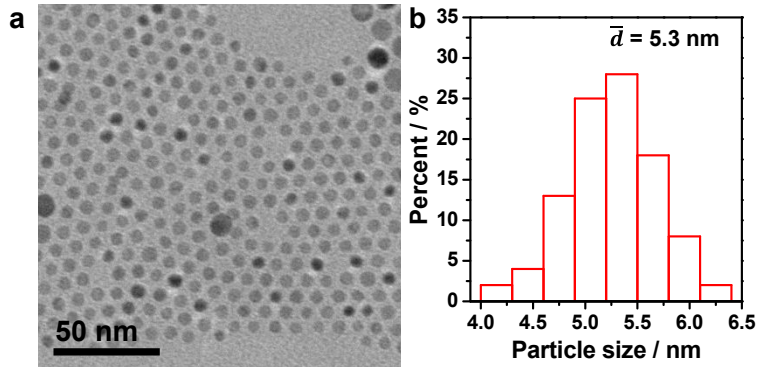

Figure S1. TEM patterns (a) and particle size distribution (b) of as-prepared PdCu nanoparticles.

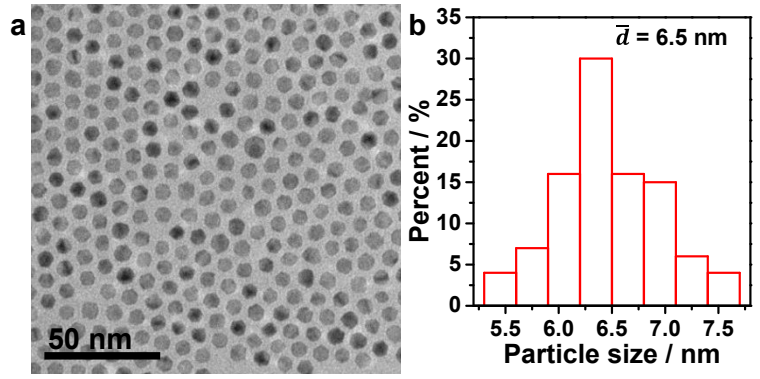

Figure S2. TEM patterns (a) and particle size distribution (b) of as-prepared Ir_{16}-PdCu nanoparticles.

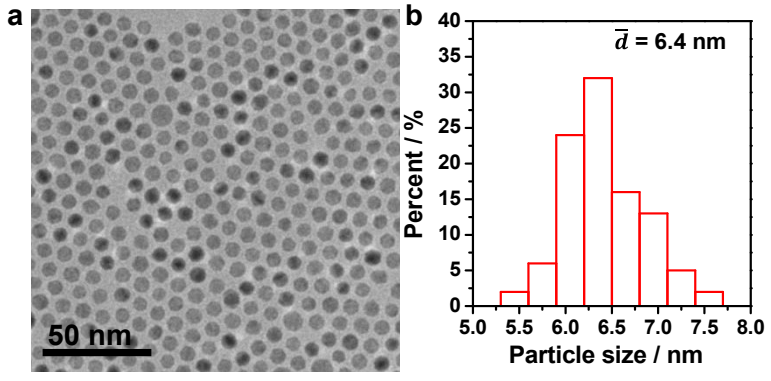

Figure S3. TEM patterns (a) and particle size distribution (b) of as-prepared Ir_8-PdCu nanoparticles.

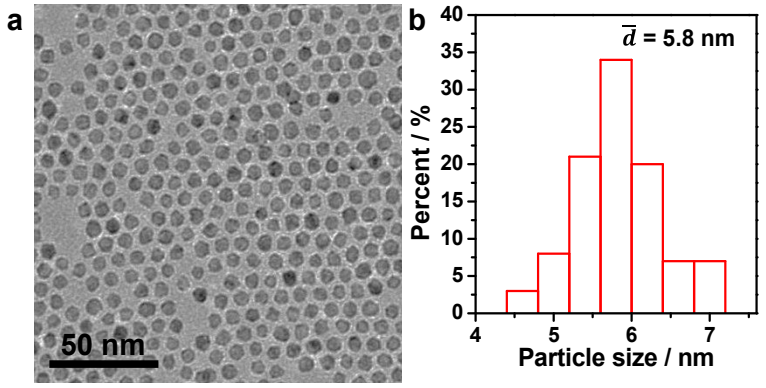

Figure S4. TEM patterns (a) and particle size distribution (b) of as-prepared Ir_{18}-PdCu nanoparticles.

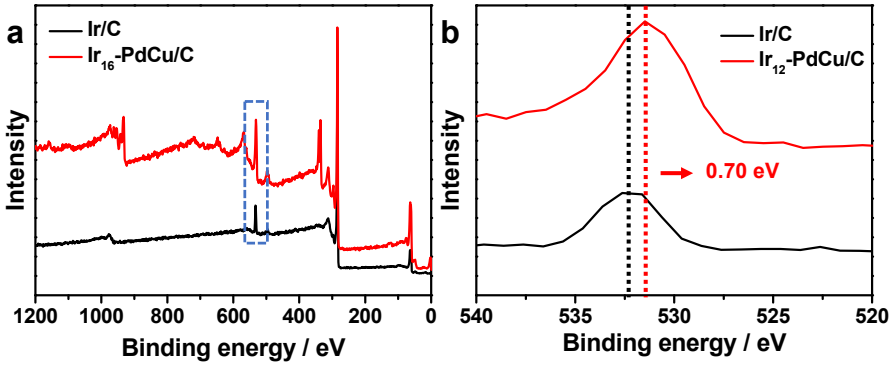

Figure S5. Comparative XPS spectrum of Ir_{16}-PdCu/C and commercial Ir/C. (a) Detailed Ir 4f spectrum. (a) Full XPS spectrums. (c) Enlargement of the dotted box in a.

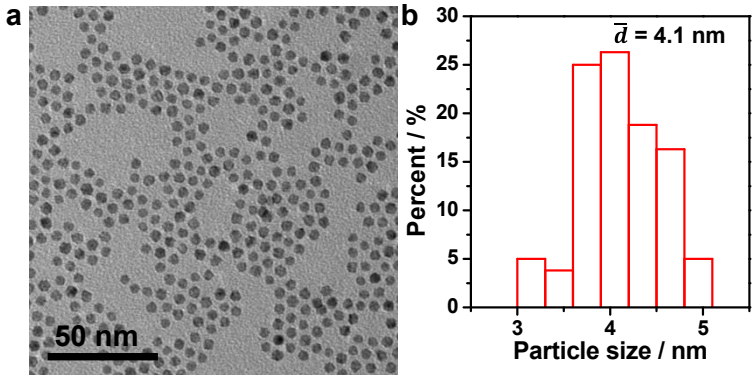

Figure S6. TEM patterns (a) and particle size distribution (b) of as-prepared PdCuIr nanoparticles synthesized without the addition of Fe^{3+}.

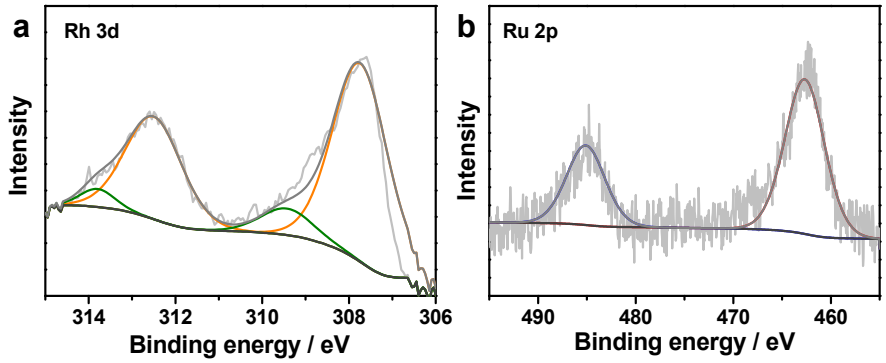

Figure S7. Detailed Rh and Ru XPS spectrum of PdCuRh/C and PdCuRu/C synthesized without Fe^{3+}. (a) Rh spectrum of PdCuRh/C. (b) Ru spectrum of PdCuRu/C.

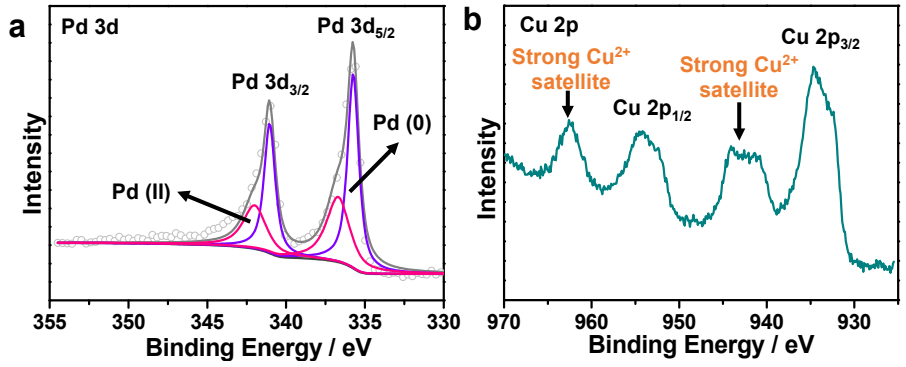

Figure S8. XPS patterns of Ir_{16}-PdCu nanoparticles. (a) Pd 3d; (b) Cu 2p.

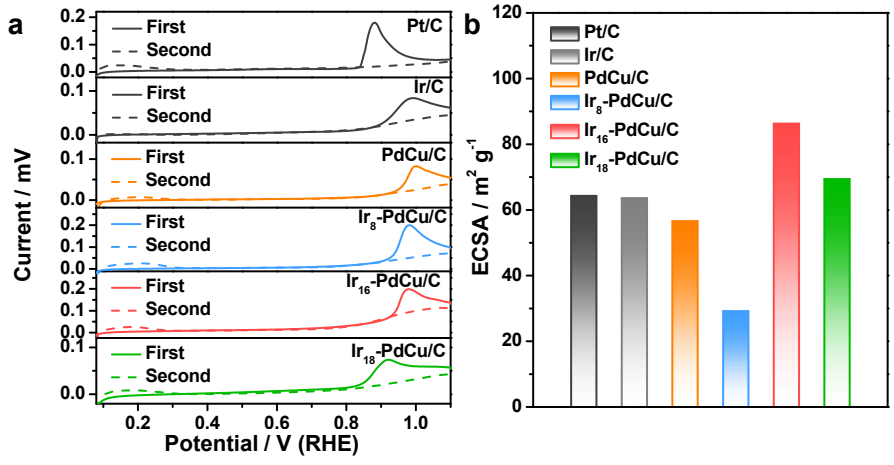

Figure S9. (a) CO stripping curves of as-prepared catalysts. (b) Corresponding ECSA calculated by CO stripping.

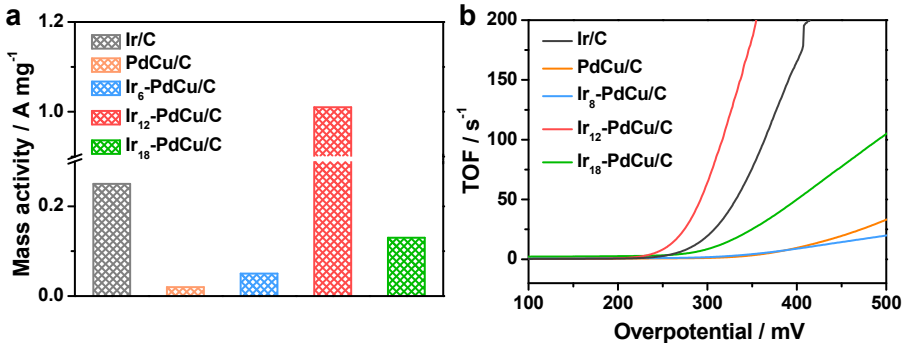

Figure S10. OER mass activity at the overpotential of 300 mV (a) and TOFs (b) of as-prepared catalysts in 0.1 M KOH.

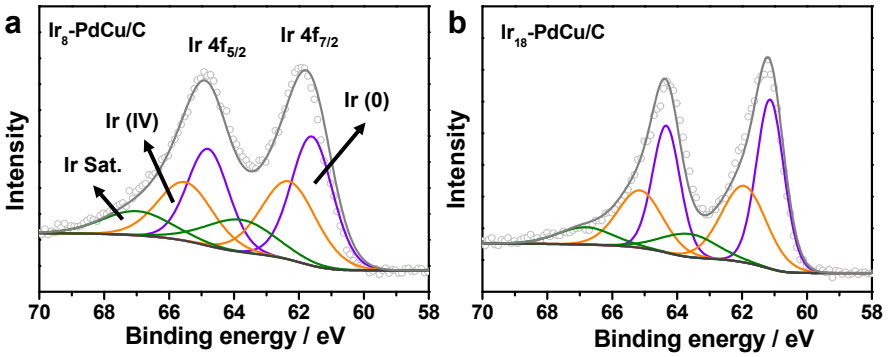

Figure S11. Detailed Ir XPS spectrum of Ir$_8$-PdCu/C and Ir$_{18}$-PdCu/C. (a) Ir$_8$-PdCu/C. (b) Ir$_{18}$-PdCu/C.

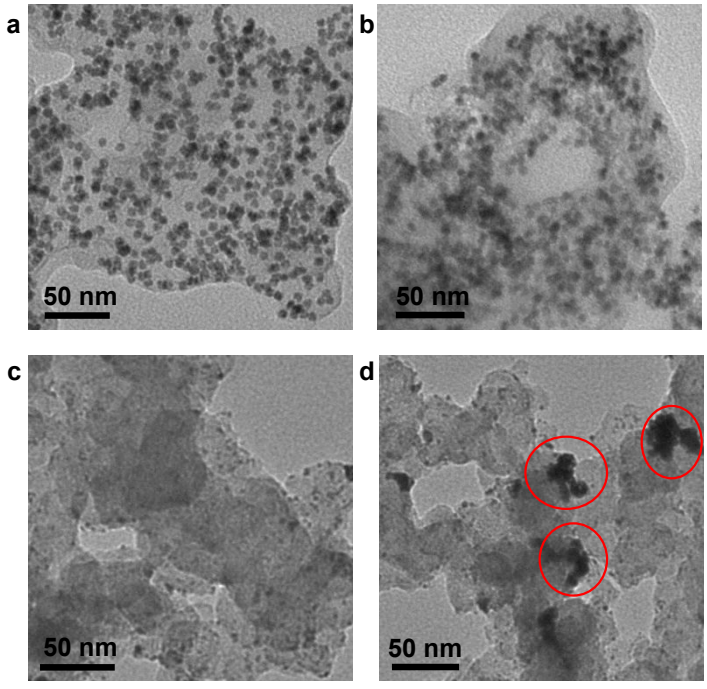

Figure S12. TEM images of Ir_{16}-PdCu/C before (a) and after (b) OER durability test, and TEM images of Pt/C before (c) and after (d) HER durability test.

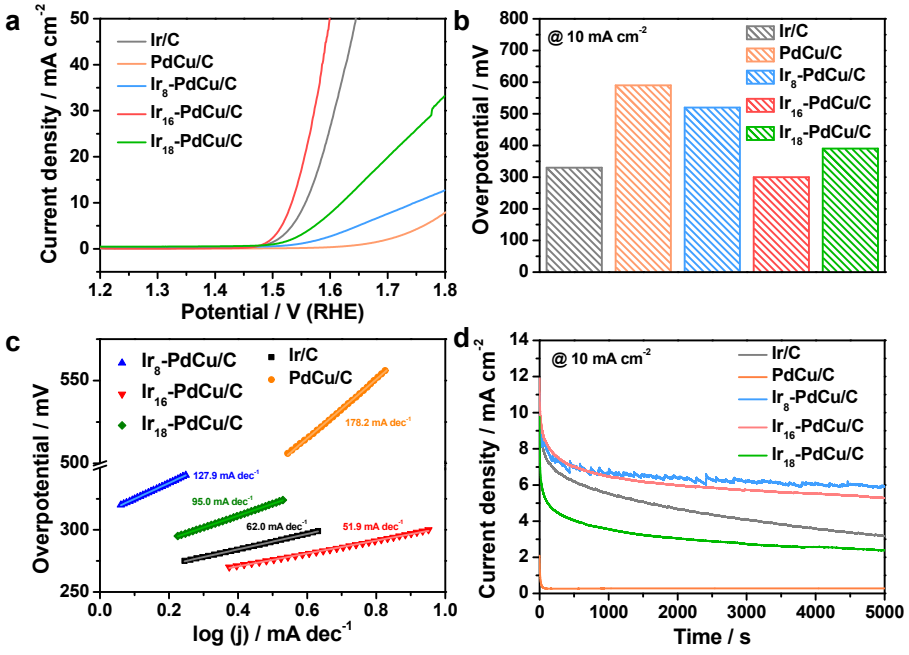

Figure S13. OER performance of Ir-PdCu and PdCu NPs in 0.1 M $HClO_4$. (a) Polarization curves with 95% iR-compensation; (b) Overpotential at the current density of 10 mA cm^{-2}; (c) Tafel slopes with 95% iR-compensation; (d) Chronoamperometry test at current densities of 10 mA cm^{-2} for 5000 s.

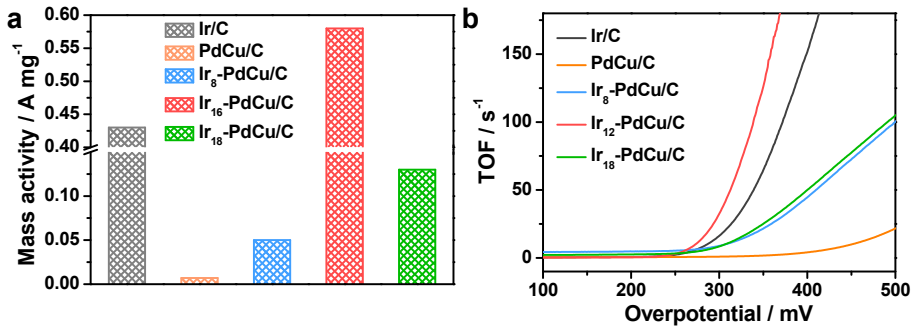

Figure S14. OER mass activity at the overpotential of 300 mV (a) and TOFs (b) of as-prepared catalysts in 0.1 M $HClO_4$.

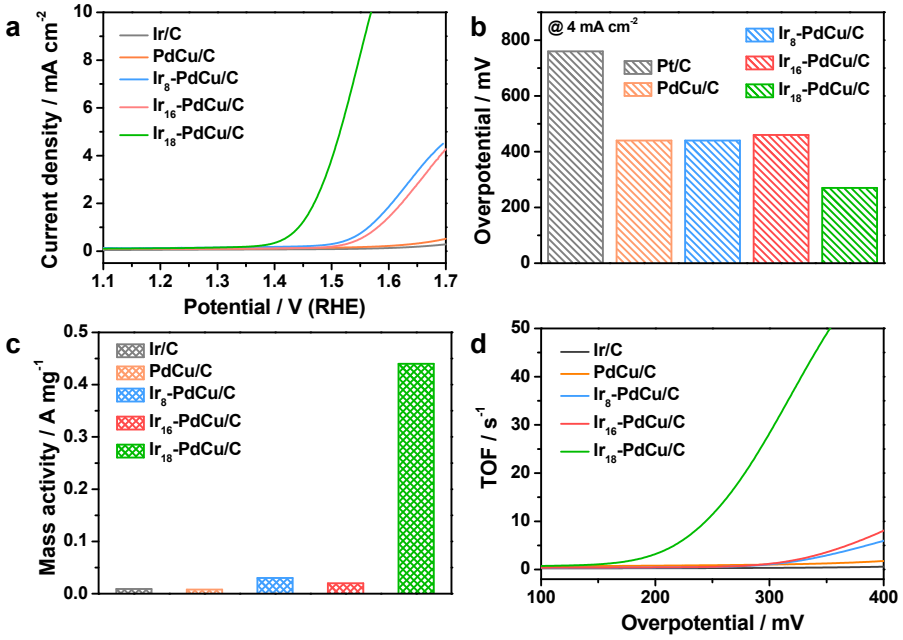

Figure S15. OER performance of Ir-PdCu and PdCu NPs in 0.1 M PBS. (a) Polarization curves with 95% iR-compensation; (b) Overpotential at the current density of 10 mA cm^{-2}; (c) HER mass activity of as-prepared catalysts in 0.1 M PBS at the overpotential of 300 mV. (d) TOF curves of as-prepared catalysts.

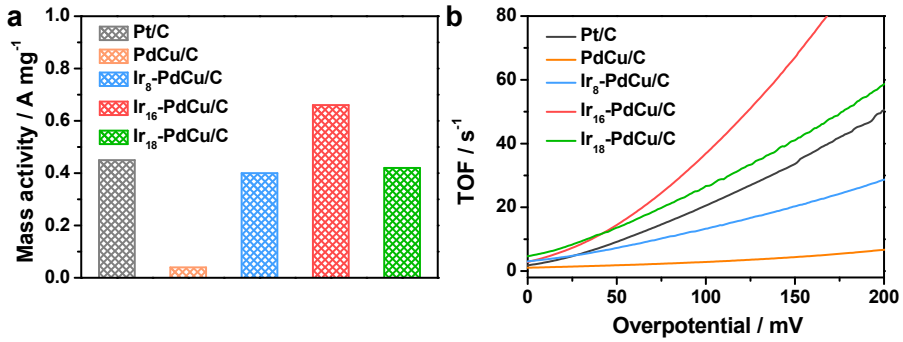

Figure S16. HER mass activity at the overpotential of 100 mV (a) and TOFs (b) of as-prepared catalysts in 0.1 M KOH.

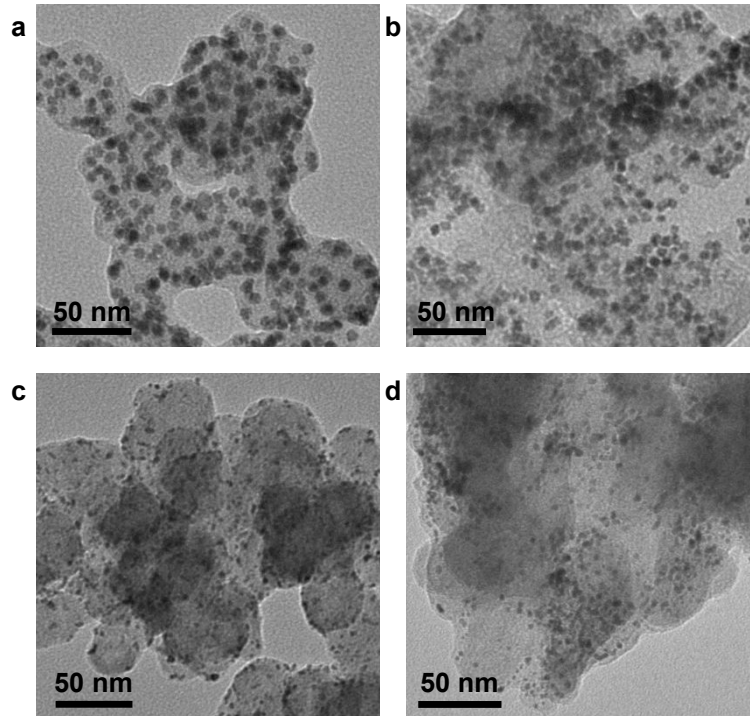

Figure S17. TEM images of Ir_{16}-PdCu/C before (a) and after (b) HER durability test, and TEM images of Ir/C before (c) and after (d) HER durability test.

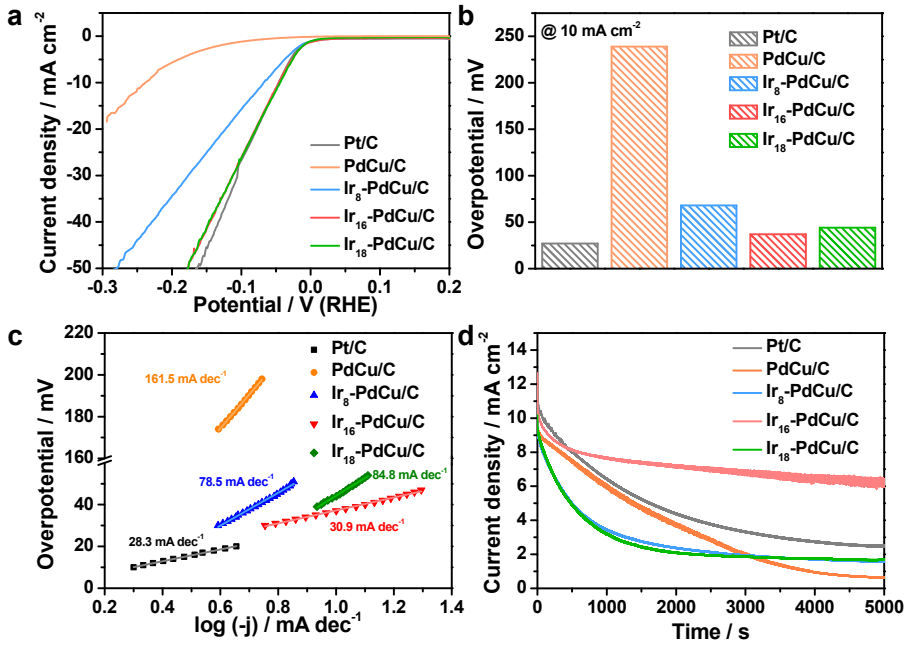

Figure S18. HER performance of Ir-PdCu and PdCu NPs in 0.1 M $HClO_4$. (a) Polarization curves with 95% iR-compensation; (b) Overpotential at the current density of 10 mA cm^{-2}; (c) Tafel slopes with 95% iR-compensation; (d) Chronoamperometry test at current densities of 10 mA cm^{-2} for 5000 s.

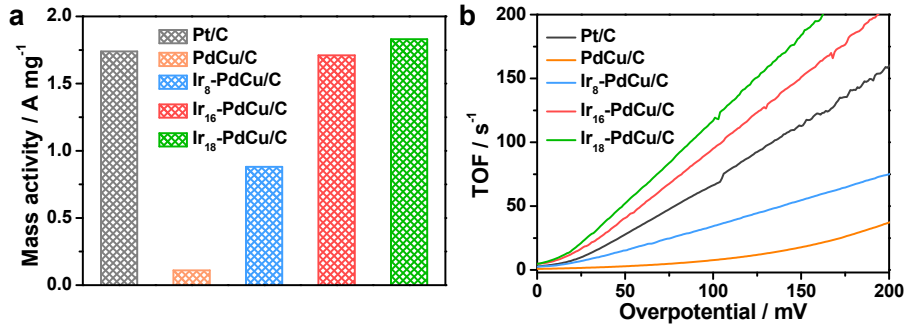

Figure S19. HER mass activity at the overpotential of 100 mV (a) and TOFs (b) of as-prepared catalysts in 0.1 M $HClO_4$.

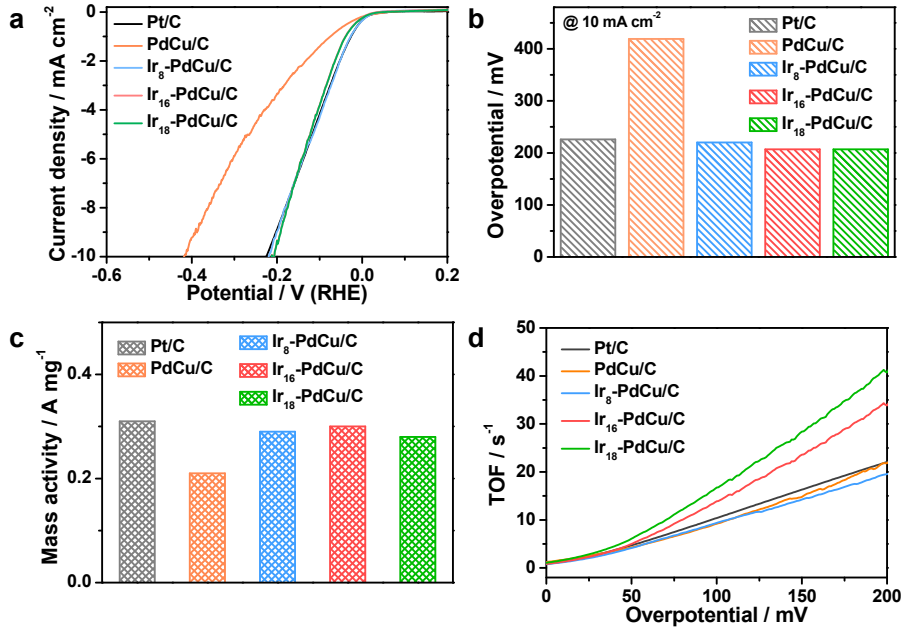

Figure S20. HER performance of Ir-PdCu and PdCu NPs in 0.1 M PBS. (a) Polarization curves with 95% iR-compensation; (b) Overpotential at the current density of 10 mA cm^{-2}; (c) HER mass activity of as-prepared catalysts in 0.1 M PBS at the overpotential of 100 mV. (d) TOF curves of as-prepared catalysts.

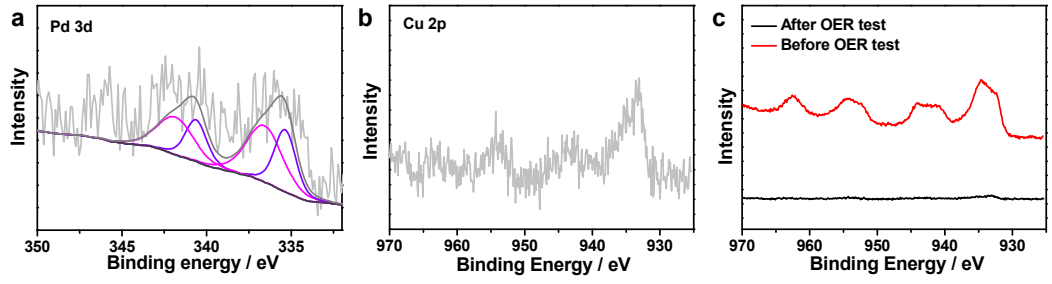

Figure S21. XPS spectrum of Ir_{16}-PdCu/C after OER stability test. (a) Detailed Pd 3d spectrum. (b) Detailed Cu 2p spectrum. (c) Comparison of Cu spectrum before and after OER test.

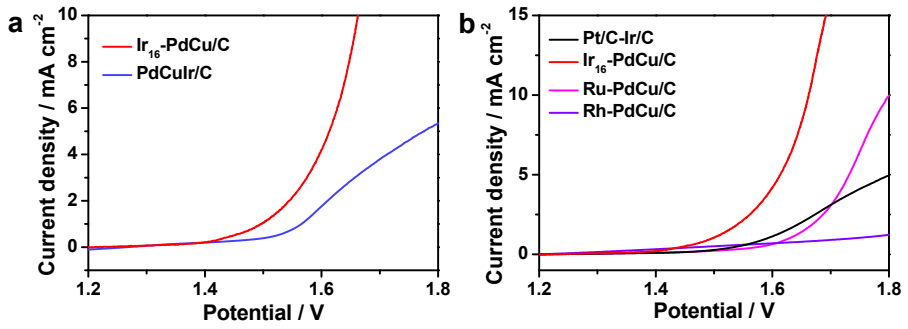

Figure S22. (a) Overall water splitting polarization curves of Ir_{16}-PdCu/C and PdCuIr/C in 0.1 M KOH at a scan rate of 5 mV/s; (b) Overall water splitting polarization curves of M-PdCu/C in 0.1 M KOH at a scan rate of 5 mV/s.

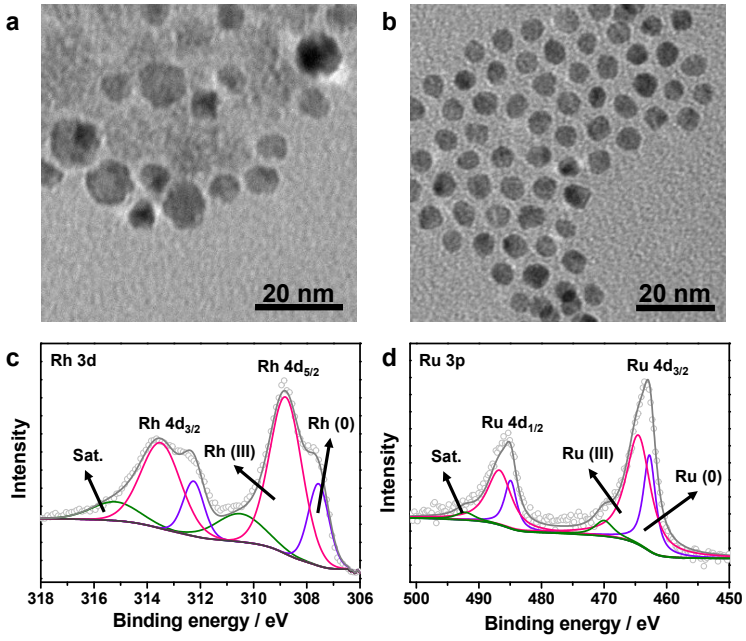

Figure S23. TEM images and XPS patterns of Rh-PdCu (a, d), Ru-PdCu (b, c).

Table S1 Metal content of as-prepared materials measured by ICP-AES.

Sample	Pd / at%	Cu / at%	Ir / at%
PdCu/C	48.5	51.5	
Ir_8-PdCu/C	50.9	41.0	8.1
Ir_{16}-PdCu/C	43.2	40.6	16.2
Ir_{18}-PdCu/C	43.0	39.2	17.8
PdCuIr	41.9	42.3	15.8

Table S2 OER TOFs of as-prepared catalysts in different electrode at 300 mV.

Sample	**$TOF_{\eta=300\ mV}$ / s^{-1}**		
	0.1 M KOH	0.1 $HClO_4$	0.1 M PBS
Ir/C	19.5	16.3	0.3
PdCu/C	1.1	0.95	1.0
Ir_8-PdCu/C	1.8	1.8	1.1
Ir_{16}-PdCu/C	64.1	32.4	1.2
Ir_{18}-PdCu/C	8.5	8.5	28.3

Table S3 HER TOFs of as-prepared catalysts in different electrode at 100 mV.

Sample	$TOF_{\eta=100\ mV}$ / s^{-1}		
	0.1 M KOH	0.1 $HClO_4$	0.1 M PBS
Pt/C	20.6	66.3	10.4
PdCu/C	2.9	7.7	9.2
Ir_8-PdCu/C	13.3	34.3	9.4
Ir_{16}-PdCu/C	36.9	95.0	13.9
Ir_{18}-PdCu/C	26.7	116.9	16.7

Table S4 Summary and comparisons of recently reported Pd/Ir-based catalysts for OER.

Sample	Electrolyte	Current density	Overpotential	References
Ir_{16}-PdCu/C	0.1 M KOH	10 mA cm^{-2}	284 mV	This work
PdP_2@CB	1.0 M KOH	10 mA cm^{-2}	270 mV	[2]
Pd@3DOM-Co_3O_4	0.1 M KOH	2 mA cm^{-2}	381 mV	[3]
PdCo-300	0.1 M KOH	10 mA cm^{-2}	350 mV	[4]
Pd_2/MoS_2	1.0 M KOH	10 mA cm^{-2}	320 mV	[5]
Pd^5Mg^{20}	1.0 M KOH	4.5 mA cm^{-2}	470 mV	[6]
Fe_2O_3/Pd	1.0 M KOH	10 mA cm^{-2}	383 mV	[7]

Pd_1@Co/NC	1.0 M KOH	10 mA cm^{-2}	470 mV	[8]
PdNiP-H	1.0 M KOH	10 mA cm^{-2}	330 mV	[9]
Ir@N-G-750	1.0 M KOH	10 mA cm^{-2}	270 mV	[10]
$Ir_{0.75}W_{0.25}$	0.1 M KOH	10 mA cm^{-2}	281 mV	[11]
Ir-NR/C	1.0 M KOH	10 mA cm^{-2}	296 mV	[12]
Ir-Pd nanotetrahedrons	1.0 M NaOH	10 mA cm^{-2}	284 mV	[13]
Ir@S–C/rGO composite	1.0 M KOH	10 mA cm^{-2}	280 mV	[14]

Table S5 Summary and comparisons of recently reported Pd/Ir-based catalysts for HER.

Sample	Electrolyte	Current density	Overpotential	References
Ir_{16}-PdCu/C	0.1 M KOH	10 mA cm^{-2}	99 mV	This work
RGO/MoS_2/Pd	1.0 M KOH	10 mA cm^{-2}	86 mV	[15]
PdNiCo@NC	1.0 M KOH	10 mA cm^{-2}	42 mV	[16]
Ir-OMC-NF	1.0 M KOH	10 mA cm^{-2}	130 mV	[17]
Ir NP/C	0.1 M KOH	10 mA cm^{-2}	79 mV	[18]
Co@Ir/NC-10%	1.0 M KOH	10 mA cm^{-2}	121 mV	[19]
Ir/Pt(poly) electrode	0.1 M NaOH	10 mA cm^{-2}	80 mV	[20]

References

[1] J. Feng, F. Lv, W. Zhang, P. Li, K. Wang, C. Yang, B. Wang, Y. Yang, J. Zhou, F. Lin, G. C. Wang, S. Guo. Iridium-Based Multimetallic Porous Hollow Nanocrystals for Efficient Overall-Water-Splitting Catalysis. *Adv. Mater.,* **2017**, *29,* 1703798.

[2] F. Luo, Q. Zhang, X. Yu, S. Xiao, Y. Ling, H. Hu, L. Guo, Z. Yang, L. Huang, W. Cai, H. Cheng. Palladium Phosphide as a Stable and Efficient Electrocatalyst for Overall Water Splitting. *Angew. Chem. Int. Ed.,* **2018**, *57*, 14862-14867.

[3] M. H. Seo, M. G. Park, D. U. Lee, X. Wang, W. Ahn, S. H. Noh, S. M. Choi, Z. P. Cano, B. Han, Z. Chen. Bifunctionally Active and Durable Hierarchically Porous Transition Metal-Based Hybrid Electrocatalyst for Rechargeable Metal-Air Batteries. *Appl. Catal. B Environ.,* **2018**, *239*, 677-687.

[4] T. Hu, Y. Wang, L. Zhang, T. Tang, H. Xiao, W. Chen, M. Zhao, J. Jia, H. Zhu. Facile synthesis of PdO-doped Co_3O_4 nanoparticles as an efficient bifunctional oxygen electrocatalyst. *Appl. Catal. B Environ.,* **2019**, *243*, 175-182.

[5] F. He, Y. Liu, Q. Cai, J. Zhao. Size-dependent electrocatalytic activity of ORR/OER on palladium nanoclusters anchored on defective MoS_2 monolayers. *New J. Chem.,* **2020**, *44*, 16135-16143.

[6] A. Datta, A. J. Porkovich, P. Kumar, G. Nikoulis, J. Kioseoglou, T. Sasaki, S. Steinhauer, P. Grammatikopoulos, M. Sowwan. Single Nanoparticle Activities in Ensemble: A Study on Pd Cluster Nanoportals for Electrochemical Oxygen Evolution Reaction. *J. Phys. Chem. C,* **2019**, *123*, 26124-26135.

[7] H. He, J. Chen, D. Zhang, F. Li, X. Chen, Y. Chen, L. Bian, Q. Wang, P. Duan, Z. Wen, X. Lv. Modulating the Electrocatalytic Performance of Palladium with the Electronic Metal–Support Interaction: A Case Study on Oxygen Evolution Reaction. *ACS Catal.,* **2018**, *8*, 6617-6626.

[8] W. H. Lai, L. F. Zhang, W. B. Hua, S. Indris, Z. C. Yan, Z. Hu, B. Zhang, Y. Liu, L. Wang, M. Liu, R. Liu, Y. X. Wang, J. Z. Wang, Z. Hu, H. K. Liu, S. L. Chou, S. X. Dou. General π-Electron-Assisted Strategy for Ir, Pt, Ru, Pd, Fe, Ni Single-Atom Electrocatalysts with Bifunctional Active Sites for Highly Efficient Water Splitting. *Angew. Chem. Int. Ed.,* **2019**, *58*, 11868-11873.

[9] S. Sankar, Y. Sugawara, S. Assa Aravindh, R. Jose, T. Tamaki, G. M. Anilkumar, T. Yamaguchi. Tuning Palladium Nickel Phosphide toward Efficient Oxygen Evolution Performance. *ACS Appl. Energy Mater.,* **2019**, *3*, 879-888.

[10] X. Wu, B. Feng, W. Li, Y. Niu, Y. Yu, S. Lu, C. Zhong, P. Liu, Z. Tian, L. Chen, W. Hu, C. M. Li. Metal-Support Interaction Boosted Electrocatalysis of Ultrasmall Iridium Nanoparticles Supported on Nitrogen Doped Graphene for Highly Efficient Water Electrolysis in Acidic and Alkaline Media. *Nano Energy,* **2019**, *62*, 117-126.

[11] L. Fu, X. Hu, Y. Li, G. Cheng, W. Luo. IrW Nanobranches as an Advanced Electrocatalyst for pH-Universal Overall Water Splitting. *Nanoscale,* **2019**, *11*, 8898-8905.

[12] F. Luo, L. Guo, Y. Xie, J. Xu, K. Qu, Z. Yang. Iridium Nanorods as a Robust and Stable Bifunctional Electrocatalyst for pH-Universal Water Splitting. *Appl. Catal. B Environ.,* **2020**, *279*, 119394.

[13] T. Zhang, S. Liao, L. Dai, J. Yu, W. Zhu, Y. Zhang. Ir-Pd Nanoalloys with Enhanced Surface-Microstructure-Sensitive Catalytic Activity for Oxygen Evolution Reaction in Acidic and Alkaline Media. *Sci. China Mater.,* **2018**, *61*, 926–938.

[14]Y. Li, Y.-Q. Zhu, W. Xin, S. Hong, X. Zhao, H. Yan, S. Xu. Interlayer Confinement Synthesis of Ir Nanodots/Dual Carbon as an Electrocatalyst for Overall Water Splitting. *J. Mater. Chem. A,* **2021**, *9*, 4176-4183.
[15]A. Pandey, A. Mukherjee, S. Chakrabarty, D. Chanda, S. Basu. Interface Engineering of an RGO/MoS_2/Pd 2D Heterostructure for Electrocatalytic Overall Water Splitting in Alkaline Medium. *ACS Appl. Mater. Interfaces,* **2019**, *11*, 42094-42103.
[16]S. Xu, F. Yang, S. Han, S. Zhang, Q. Wang, C. Jiang. MOF-derived PdNiCo Alloys Encapsulated in Nitrogen-Doped Graphene for Robust Hydrogen Evolution Reactions. *CrystEngComm,* **2020**, *22*, 6063-6070.
[17]Y. H. He, J. M. Xu, F. N. Wang, X. C. Zhao, G. Z. Yin, Q. Mao, Y. Q. Huang, T. Zhang. In-Situ Carbonization Approach for the Binder-Free Ir-Dispersed Ordered Mesoporous Carbon Hydrogen Evolution Electrode. *J. Energy Chem.,* **2017**, *26*, 1140-1146.
[18]F. Yang, L. Fu, G. Cheng, S. Chen, W. Luo. Ir-Oriented Nanocrystalline Assemblies with High Activity for Hydrogen Oxidation/Evolution Reactions in an Alkaline Electrolyte. *J. Mater. Chem. A,* **2017**, *5*, 22959-22963.
[19]D. Li, Z. Zong, Z. Tang, Z. Liu, S. Chen, Y. Tian, X. Wang. Total Water Splitting Catalyzed by Co@Ir Core–Shell Nanoparticles Encapsulated in Nitrogen-Doped Porous Carbon Derived from Metal–Organic Frameworks. *ACS Sustainable Chem. Eng.,* **2018**, *6*, 5105-5114.
[20]S. Strbac, M. Smiljani, T. Wakelin, J. P. cnik, Z. Rakocevic. Hydrogen Evolution Reaction on Bimetallic Ir/Pt(Poly) Electrodes in Alkaline Solution. *Electrochim. Acta,* **2019**, *306*, 18-27.